Ultra-low loss ridge waveguides on lithium niobate via argon ion milling and gas clustered ion beam smoothening

Shawn Yohanes Siew, Eric Jun Hao Cheung, Haidong Liang, Andrew Bettiol, Noriaki Toyoda, Bandar Alshehri, El Hadj Dogheche, Aaron J. Danner

Research Article | Vol. 26, No. 4 | 19 Feb 2018 | OPTICS EXPRESS 4421
Optics EXPRESS

Ultra-low loss ridge waveguides on lithium niobate via argon ion milling and gas clustered ion beam smoothening

SHAWN YOHANES SIEW,[1] ERIC JUN HAO CHEUNG,[1] HAIDONG LIANG,[2] ANDREW BETTIOL,[2] NORIAKI TOYODA,[3] BANDAR ALSHEHRI,[4] ELHADJ DOGHECHE,[4] AND AARON J. DANNER[1,*]

[1]*Department of Electrical and Computer Engineering, National University of Singapore, 4 Engineering Drive 3, 117583, Singapore*
[2]*Department of Physics, National University of Singapore, 2 Science Drive 3, 117551, Singapore*
[3]*Department of Electronics and Computer Science, Graduate School of Engineering, University of Hyogo, Japan*
[4]*Institute of Electronic, Microelectronics, and Nanotechnology, IEMN DOAE, University of Valenciennes, 59309 Valenciennes, France*
**adanner@nus.edu.sg*

Abstract: Lithium niobate's use in integrated optics is somewhat hampered by the lack of a capability to create low loss waveguides with strong lateral index confinement. Thin film single crystal lithium niobate is a promising platform for future applications in integrated optics due to the availability of a strong electro-optic effect in this material coupled with the possibility of strong vertical index confinement. However, sidewalls of etched waveguides are typically rough in most etching procedures, exacerbating propagation losses. In this paper, we propose a fabrication method that creates significantly smoother ridge waveguides. This involves argon ion milling and subsequent gas clustered ion beam smoothening. We have fabricated and characterized ultra-low loss waveguides with this technique, with propagation losses as low as 0.3 dB/cm at 1.55 μm.

OCIS codes: (130.0130) Integrated optics; (190.0190) Nonlinear optics; (220.0220) Optical design and fabrication; (230.7370) Waveguides.

References and links

1. R. L. Byer, J. F. Young, and R. S. Feigelson, "Growth of High-Quality LiNbO3 Crystals from the Congruent Melt," J. Appl. Phys. **41**(6), 2320–2325 (1970).
2. Y.-S. Lee, T. Meade, V. Perlin, H. Winful, T. B. Norris, and A. Galvanauskas, "Generation of narrow-band terahertz radiation via optical rectification of femtosecond pulses in periodically poled lithium niobate," Appl. Phys. Lett. **76**(18), 2505–2507 (2000).
3. C. Campbell, *Surface Acoustic Wave Devices for Mobile and Wireless Communications* (Academic Press, Inc., 1998).
4. M. Levy, R. Liu, L. E. Cross, A. Kumar, and H. Bakhru, "Fabrication of single-crystal lithium niobate films by crystal ion slicing," Appl. Phys. Lett. **73**(16), 2293–2295 (1998).
5. A. Guarino, G. Poberaj, D. Rezzonico, R. Degl'Innocenti, and P. Günter, "Electro-optically tunable microring resonators in lithium niobate," Nat. Photonics **1**(7), 407–410 (2007).
6. P. Rabiei, J. Ma, S. Khan, J. Chiles, and S. Fathpour, "Heterogeneous lithium niobate photonics on silicon substrates," Opt. Express **21**(21), 25573–25581 (2013).
7. N. Courjal, B. Guichardaz, G. Ulliac, J.-Y. Rauch, H.-H. Lu, S. Benattou, and M.-P. Bernal, "High aspect ratio lithium niobate ridge waveguides fabricated by optical grade dicing," J. Phys. D Appl. Phys. **44**(30), 305101 (2011).
8. F. Lenzini, S. Kasture, B. Haylock, and M. Lobino, "Anisotropic model for the fabrication of annealed and reverse proton exchanged waveguides in congruent lithium niobate," Opt. Express **23**(2), 1748–1756 (2015).
9. D. H. Jundt, "Temperature-dependent Sellmeier equation for the index of refraction, ne, in congruent lithium niobate," Opt. Lett. **22**(20), 1553–1555 (1997).
10. L. A. Coldren, S. C. Nicholes, L. Johansson, S. Ristic, R. S. Guzzon, E. J. Norberg, and U. Krishnamachari, "High Performance InP-Based Photonic ICs," J. Lightwave Technol. **29**(4), 554–570 (2011).

#312564 https://doi.org/10.1364/OE.26.004421
Journal © 2018 Received 2 Nov 2017; revised 26 Dec 2017; accepted 27 Dec 2017; published 9 Feb 2018

Optics EXPRESS

11. T. Z. U. Fischer, J. R. Kropp, F. Arndt, and K. Petermann, "0.1 dB/cm waveguide losses in single-mode SOI rib waveguides," IEEE Photonics Technol. Lett. **8**(5), 647–648 (1996).
12. S. Y. Siew, S. S. Saha, M. Tsang, and A. J. Danner, "Rib Microring Resonators in Lithium Niobate on Insulator," IEEE Photonics Technol. Lett. **28**(5), 573–576 (2016).
13. S. Y. Siew, E. J. H. Cheung, M. Tsang, and A. J. Danner, "Integrated nonlinear optics: lithium niobate-on-insulator waveguides and resonators," in *SPIE OPTO*, (SPIE, 2017), 8.
14. I. Yamada and N. Toyoda, "Summary of recent research on gas cluster ion beam process technology," Nuclear Instrum. Methods Phys. Res. Section B **232**(1-4), 195–199 (2005).
15. E. J. Teo, N. Toyoda, C. Yang, A. A. Bettiol, and J. H. Teng, "Nanoscale smoothing of plasmonic films and structures using gas cluster ion beam irradiation," Appl. Phys., A Mater. Sci. Process. **117**(2), 719–723 (2014).
16. A. Gerthoffer, C. Guyot, W. Qiu, A. Ndao, M.-P. Bernal, and N. Courjal, "Strong reduction of propagation losses in LiNbO3 ridge waveguides," Opt. Mater. **38**, 37–41 (2014).
17. R. G. Walker, "Simple and accurate loss measurement technique for semiconductor optical waveguides," Electron. Lett. **21**(13), 581–583 (1985).
18. S. Y. Siew, E. J. H. Cheung, M. Tsang, and A. J. Danner, "Loss characterization of waveguides in lithium niobate on insulator," in *2016 International Conference on Optical MEMS and Nanophotonics (OMN)* (2016), pp. 1–2.
19. S. Li, L. Cai, Y. Wang, Y. Jiang, and H. Hu, "Waveguides consisting of single-crystal lithium niobate thin film and oxidized titanium stripe," Opt. Express **23**(19), 24212–24219 (2015).
20. T. Keisuke and S. Toshiaki, "Fabrication of 0.7 μm 2 ridge waveguide in ion-sliced LiNbO 3 by proton-exchange accelerated chemical etching," Jpn. J. Appl. Phys. **54**(12), 128002 (2015).
21. G. Ulliac, V. Calero, A. Ndao, F. I. Baida, and M. P. Bernal, "Argon plasma inductively coupled plasma reactive ion etching study for smooth sidewall thin film lithium niobate waveguide application," Opt. Mater. **53**, 1–5 (2016).
22. M. F. Volk, S. Suntsov, C. E. Rüter, and D. Kip, "Low loss ridge waveguides in lithium niobate thin films by optical grade diamond blade dicing," Opt. Express **24**(2), 1386–1391 (2016).

1. Introduction

Single crystal lithium niobate is a commercially important nonlinear optical crystal. It can be grown with high quality [1] and has unique nonlinear electro-optic effects that arise from its inherently strong 2nd order electrical field susceptibility (or χ^2 nonlinear coefficient). Useful χ^2 effects include the Pockels effect (used for linear electro-optical modulation), sum frequency generation (for wavelength changing), optical rectification (for generation of terahertz waves [2]) and spontaneous parametric down-conversion (potentially of use in quantum optics). Additionally, lithium niobate demonstrates very useful surface acoustic wave (SAW) effects due to its acoustic and piezoelectric properties [3]. As a result, lithium niobate has found widespread commercial use in modulators, sensors and also SAW devices.

To create waveguiding conditions in lithium niobate, conventionally, titanium indiffusion or proton exchange is used. In these methods, at high temperatures, ions are diffused into a targeted region of lithium niobate, changing the stoichiometric composition and nominally increasing the refractive index there. Both diffusion methods tend not to result in a large associated index increase, and in the case of proton exchange, a decrease in refractive index along one axis results (lithium niobate being birefringent). Although the resultant increase in index along at least one axis can yield robust and low-loss waveguiding, for waveguide turns very large turning radii are needed to guide light and avoid bending loss; this somewhat hampers lithium niobate's utility in integrated optics applications and useful devices tend to be on the order of millimeters in dimension. Strongly confined etched waveguides can potentially solve this problem, if the propagation loss can be made as low as that in weakly confined diffused waveguides.

Thin film single crystal lithium niobate or lithium-niobate-on-insulator (LNOI) [4] is a promising platform for pursuing this goal and essentially solves the problem of vertical index confinement; this is similar to the silicon-on-insulator (SOI) approach, and the resultant structure is an optically thin film (sub-micron) of single crystal lithium niobate wafer-bonded to a lower-index layer (typically silicon dioxide) grown on top of a substrate. Strong confinement in waveguides is provided vertically via the silicon dioxide layer below, and laterally via dry etching. However, due to the nature of lithium niobate, etched sidewalls in practically all reported studies till now tend to suffer from rather serious sidewall roughness

Optics EXPRESS

exacerbating propagation losses. For example, A. Guarino et al. initial work [5] have achieved 17 dB/cm in a waveguide etched with dry etching methods; P. Rabiei et al. [6] improved the processes and achieved 5 dB/cm in etched waveguides; N. Courjal et al. [7] have achieved 0.5 dB/cm albeit with Ti-indiffused ridge waveguides. For comparison, typical propagation losses in industrially-relevant Ti-diffused waveguides tend to be as low as 0.086 dB/cm [8].

In this paper, we propose a two-step fabrication method that yields much lower propagation losses than in single-step dry etches. The process involves optimized argon ion milling and subsequent gas clustered ion beam smoothening, both which work in concert to reduce the sidewall roughness. We have fabricated and characterized ultra-low loss waveguides (< 1 dB/cm) made by this technique. The low loss coupled with the capability for sharp bending radii/strong index confinement makes this method useful in the development of future photonic integrated circuits in this platform.

2. Methodology

A Z-cut LNOI wafer fabricated via crystal ion slicing and wafer bonding was first obtained from a commercial supplier. The configuration is shown in Fig. 1 with h = 700 nm. We varied the width w of the waveguide from 1 μm to 7 μm. This width refers to the width of the etch mask, and due to etching processes, the sidewalls tend to be angled. As a result, the base of the waveguide tends to be slightly larger than w.

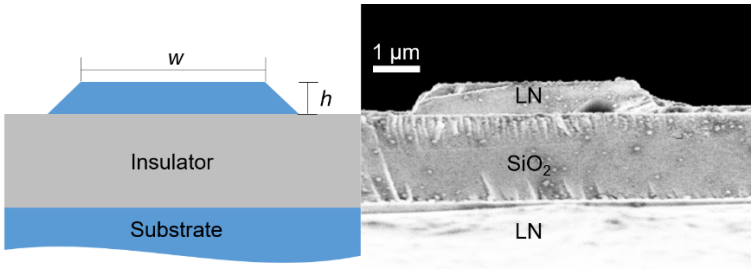

Fig. 1. Ridge waveguide structure. The blue regions represent single crystal lithium niobate. The width w of the waveguide is experimentally varied from 1 μm to 7 μm, whereas the height h is fixed at 700 nm. Due to etching processes, the sidewall tends to have an angle.

Refractive indices provided by substrate supplier are n_o = 2.211 and n_e = 2.138 at 1550 nm wavelength. As the crystal ion slicing process can potentially cause crystal damage, we measured these indices using the prism coupling method, and found n_o = 2.204 ± 0.004 and n_e = 2.155 ± 0.013 at 1539 nm, which agrees well with values reported in literature [9].

These refractive index values are subsequently used to calculate mode profiles given the geometry, using a finite element solver (COMSOL). Since the sidewalls tend to be sloped, we simulated both the straight cases and angled cases. For a fair comparison, the height is fixed but the total area of the waveguide is kept the same for both cases. Therefore the width of the straight case will equal to the average of the top and bottom width of the angled case. Figure 2 shows the case of w = 2 μm. The mode profiles of the angle case and straight case are fairly similar as expected for the TE0 and TM0 modes, but results increasingly differ for higher order modes. This is because the fields of higher order modes congregate near the sidewalls significantly more than those of the fundamental mode. As long as the waveguides are single mode (or nearly so), these results show intuitively that the sidewall slope is an insignificant concern.

Optics EXPRESS

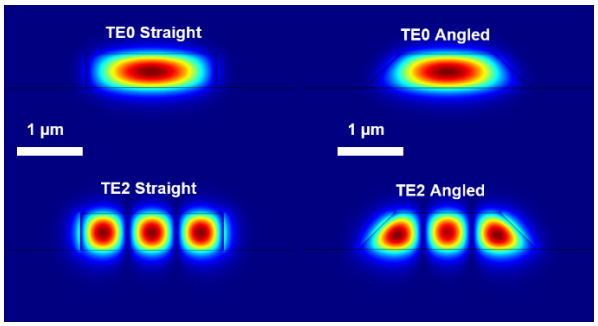

Fig. 2. Theoretical TE mode profiles solved via finite element solving in COMSOL. On the right shows an angled waveguide with an angle of 45 degrees and a top waveguide width of 2 μm. On the right shows an equivalent "straight" waveguide with the same area. The top represents the TE0 mode, whereas the bottom represents the TE mode.

In fact, higher order modes tend to have increasing field overlap with the cladding material and sidewalls. The effective refractive indices for the first three modes are plotted in Fig. 3. Although these simulations can estimate the effective index of higher order modes at small waveguide widths, these modes tend not to be supported but are included here for completeness. The open data points in Fig. 3 represent the straight waveguide case, and the solid data points represent the sloped waveguide case. Generally, there is a slight difference in effective index that only becomes pronounced when the mode is more tightly squeezed laterally. As a result, we conclude that this angled sidewall is not a disadvantage given the single mode behavior of our waveguides.

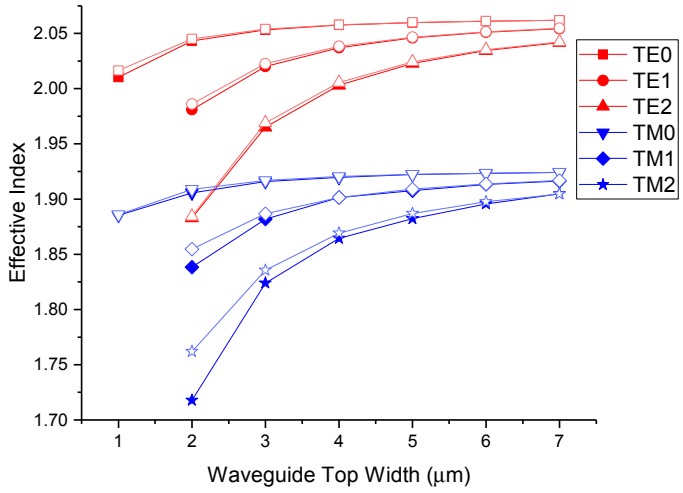

Fig. 3. Simulated effective refractive index depending upon the geometry of the waveguide for the first few TE & TM modes. The closed symbols represent the "angled" case, whereas the open symbols represent the "straight" case. The results are very similar for the fundamental modes.

The fabrication process is as follows:

1. A Z-cut LNOI wafer is diced into 1.2 cm x 1 cm pieces, with the long edge aligned with the crystal Y axis. The sample is cleaned with acetone and isopropanol.

Optics EXPRESS

2. 100 nm of Cr is deposited with electron beam evaporation. This layer serves to prevent charging and acts as a hard mask.
3. 300 nm of ma-N 2403 negative resist is spin coated onto the substrate, and patterned with electron beam lithography. A stage moving exposure technique (fixed beam moving stage) is utilized to prevent stitching errors. The resist is developed and subsequently post-baked.
4. After development, a nitric acid based etchant is used to remove the exposed Cr. Subsequently, argon ion milling is used to etch 700 nm of the lithium niobate ridge. The resist and chromium both act as a hard mask.
5. Remaining resist is removed via acetone, and subsequently any remaining Cr is removed with nitric acid based Cr etchant.
6. To remove the resist bead at the end of the sample, an additional 0.5 mm is diced off each end of the waveguides using a diamond saw dicer. The end facets of the waveguides are polished with an Ar focused ion beam to facilitate end facet coupling.
7. The sample is characterized, and subsequently gas clustered ion beam is used as described below to further smoothen the sidewall.

Lithium niobate is known to be notoriously difficult to dry etch which typically leads to very rough sidewalls. This is evident in the significantly higher loss of etched waveguides in lithium niobate compared to competing platforms such as silicon and indium phosphide, which can be as low as 0.1 dB/cm [10, 11]. As such, to obtain a smooth sidewall, it is important to calibrate and optimize all steps of the process, particularly the etching processes. Argon ion milling is ideal [12] for this purpose. Previously we have explored inductively coupled plasma, but found that the reactive gas used (fluorine) tended to react with the sidewalls and redeposit a lithium fluoride compound, which is even more difficult to etch. Physical etching however does not suffer from this problem. However, re-deposition at the sidewalls still occurs and this leads to an angled sidewall. The argon ion milling setup is shown in Fig. 4. The sample holder is rotated to improve uniformity of etching.

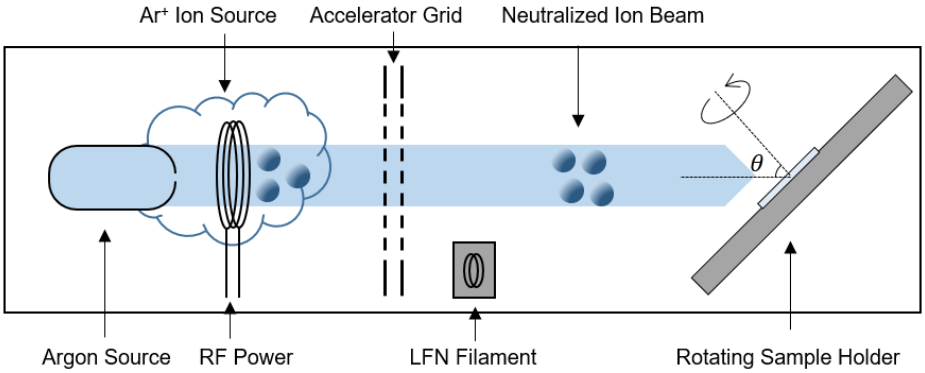

Fig. 4. Argon ion milling setup. Argon ions are first striped of their electron using RF power, and subsequently accelerated via a ion optics grid. Before striking the sample, the argon ions are neutralized with a lower filament neutralizer (LFN) which helps to prevent charging of the sample.

The argon ion milling process results in a sidewall angle of approximately 45°. The (masked) wafer is first milled at an angle 7° off normal under continuous rotation, utilizing a high beam power to define the features, which produces steep but comparatively rough sidewalls. The etch rate is approximately 17 nm per min, so 680 nm requires 40 min of

Optics EXPRESS

milling. Subsequently, a significantly lower power is used for 3 min at 60° off normal, which serves as an intermediate smoothening step. This step serves to allow the sidewall to be directly attacked by the ion beam, and we have noticed an improvement in the roughness via SEM after this step. The remaining 20 nm of thin film lithium niobate is etched away at the same time. The argon ion milling process parameters have been previously detailed in [13].

Subsequently, gas clustered ion beam has been used to further smoothen the sidewalls. The device is mounted at an angle. Using an analyzing magnet, monomer ions are filtered out of an Ar ion source. This forms a ball of argon ions many nanometers in diameter, which is accelerated to bombard the ions [14]. Due to the larger mass of the argon ion cluster, this provides a smoothing action [15]. The machine setup is shown in Fig. 5. The samples are mounted at an angle to provide better access to the sidewalls. We believe this group of steps provides the best smoothness possible using purely physical methods.

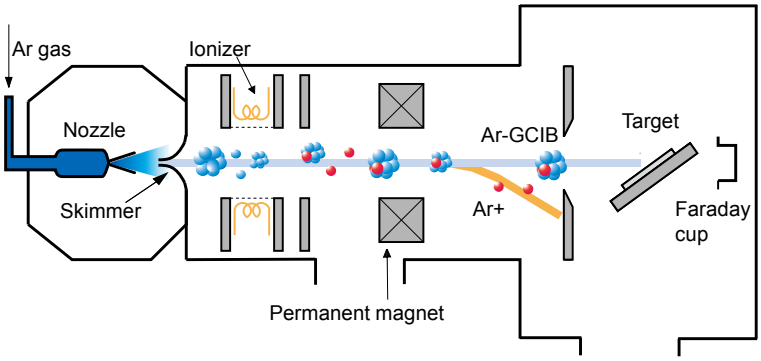

Fig. 5. Gas Clustered Ion Beam smoothening setup. It is similar to conventional argon ion milling, but with a modified argon source, includes an analysis magnet to filter out monomer beams and only accelerates clusters of chosen sizes.

3. Characterization

The effects of GCIB smoothening are evident in scanning electron microscopy images (SEM) as shown in Fig. 6. The sample is mounted at a slight angle to enable the sidewall to be viewed. There is clear smoothening action due to the GCIB process.

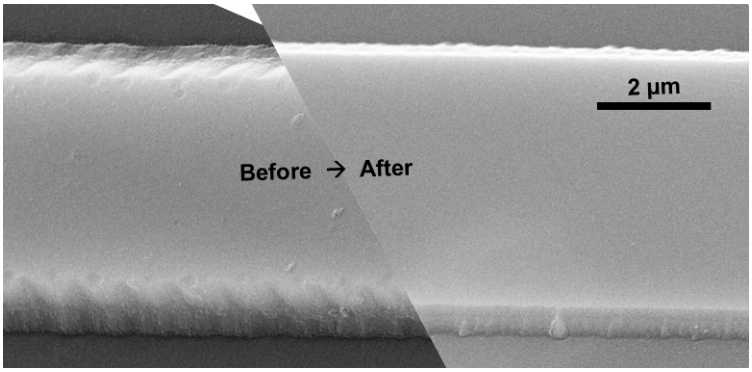

Fig. 6. SEM images of a 5 µm waveguide showing before and after the GCIB operation.

We also used atomic form microscopy (AFM) to measure the roughness of the sidewall after GCIB etching, as shown in Fig. 7. Figure 7(a) shows the AFM measurement of a large (5 by 5 microns), but the roughness calculation is performed on a smaller, higher resolution range (800 by 800 nanometers) after performing a 1st order flattening to remove the sidewall slope. The measured RMS roughness is around 8 nm. However, because of the high slope of the sidewall, the measurement may not be accurate.

Optics EXPRESS

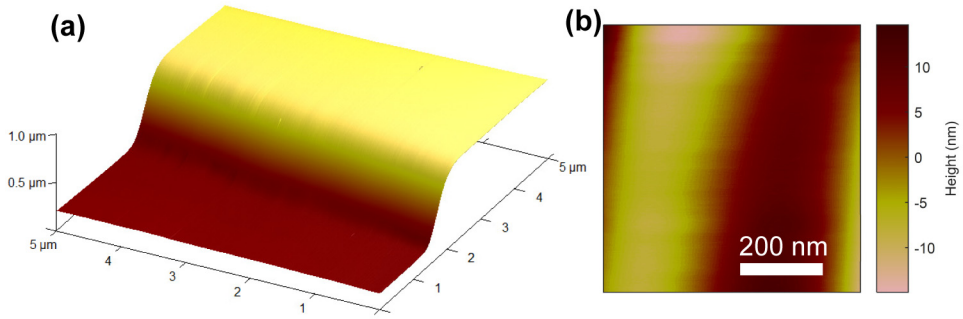

Fig. 7. (a) AFM of the side of the a 5 μm waveguide, with (b) showing a zoomed in view (with a 1st order flatten). The measured roughness over the whole of (b) of Rq is 8.3 nm and Ra is 6.9 nm.

To measure the loss, we used a Fabry Perot resonance calculation method. The waveguide can be considered as a cavity with each end facet of the waveguide acting as a mirror. This can be exploited to calculate the loss from the transmission and reflection spectra. We characterized the transmission spectra using a tunable laser and a detector. By including an optical circulator we can simultaneously measure the transmission and reflection spectrum of these waveguides. Since our waveguide is 1.2 cm long, we expect resonances to be 45 pm apart. Thus, we used a resolution of 1 pm increments to measure the FP resonances.

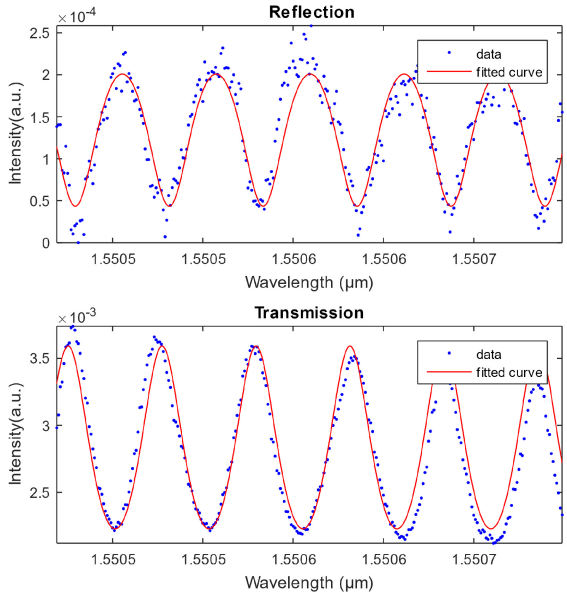

Fig. 8. Transmission and reflection (TE) spectra at 1,550 nm of a 7 μm waveguide, showing the fitted curve.

The transmission and reflection spectra are theoretically derived as per (1) [16]

$$\frac{I_{transmission}}{I_{initial}} = \frac{(1-R)^2 G}{(1-RG)^2 + 4RG\sin^2(\delta/2)}$$
$$\frac{I_{reflection}}{I_{initial}} = \frac{R(1-G)^2 + 4RG\sin^2(\delta/2)}{(1-RG)^2 + 4RG\sin^2(\delta/2)}, \quad (1)$$

Optics EXPRESS

where R is the reflectivity (equal to $r_1 r_2$), G is the gain of the cavity, expressed as $\exp(-\alpha L)$, wherein L is the length of the sample) and δ is the phase difference of successive reflections (expressed as $4\pi nL/\lambda$). It can be seen from (1) that the cavity gain (synonymous to propagation loss in this case) can be derived as (2) from the transmission spectrum [17].

$$\alpha = \frac{1}{L}\ln\left(R\frac{1+\zeta}{1-\zeta}\right), \tag{2}$$

where ζ refers to the ratio between the maximum transmission intensity and the minimum transmission intensity. Therefore, we can simultaneously fit both the reflection and transmission spectra to obtain estimates for R and G, thereby estimating the loss from without the need to assume the reflection coefficient. The TE results are shown in Fig. 8. Fitting the data for a 7 μm waveguide shows an end facet reflection 12.5% and a loss of 0.268 dB/cm, with an r-square error of 0.823 and 0.919 for the reflection and transmission case, respectively. We used this method to calculate the propagation losses for various waveguides of various w to produce Fig. 9. Notably, TM losses tend to be higher especially at smaller w; this is due to a weaker confinement (the birefringence of lithium niobate is around 0.08) and because TM modes tend to be more susceptible to roughness. Since we used the least absolute residual method for fitting in MATLAB when we bound the other variables, it is possible to obtain a confidence interval for the gain variable G. Where appropriate, error bars are extracted from the confidence interval of fitting of both the reflection and transmission spectra. Since we fit the gain variable $G = \exp(-\alpha L)$, the error bars are asymmetric when expressed in dB/cm units. When the waveguide width w tends to smaller dimensions, the data (especially for the TM polarization) becomes less clear, resulting in a larger error bar. The results show that our processes induce a notable improvement in propagation loss over other reported in literature. It should also be pointed out that we have previously compared this method of loss estimation with both a method based on use of an IR camera capturing scattered light from above and a cutback-like method [18] and found robust agreement.

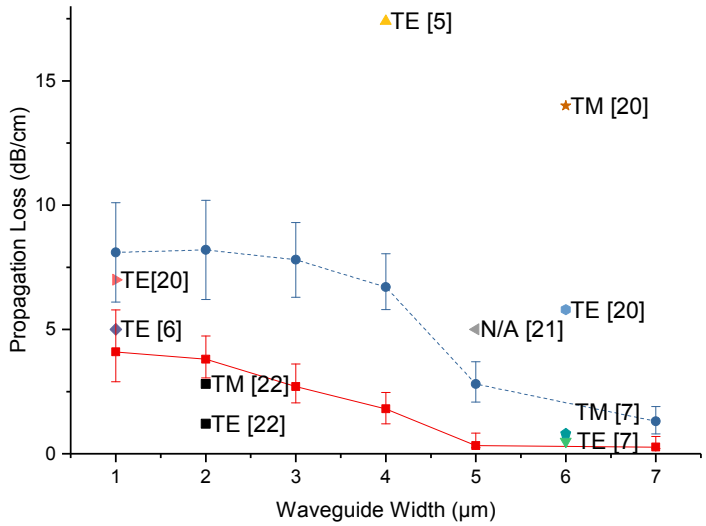

Fig. 9. Propagation loss vs Waveguide Width for both TE and TM, calculated via Fabry Perot resonance measurement data. Other results in literature are indicated, and the polarization from these results are indicated if available.

Optics EXPRESS

4. Conclusion

In Table 1, we have compared our results with other loss values of etched or diced thin film waveguides in contemporary literature. Although different fabrication methods have their own strengths and weaknesses, it is clear that the method we have described here compares favorably in terms of propagation loss (our waveguides were also relatively deeply etched at 700 nm, whereas many waveguides in Table 1 are etched to a shallower extent). Notably, our method compares favorably to both optical grade dicing and grown waveguides, however these fabrication methods come at a price of additional fabrication complexity and/or constraints. Since our proposed methods do not add significant fabrication steps and produce very good results, we are hopeful about extending this method to other materials systems as well.

Table 1. Comparison of Thin Film Lithium Niobate Waveguides

Waveguide Type	Propagation Loss (dB/cm)	Waveguide Width (μm)	Source
Etched Rib Waveguide (400 nm etched)	17.4	4	2007 [5]
Ti-indiffused Ridge Waveguides	0.5 (TE) 0.8 (TM)	6 (top width)	2011 [7]
Ta_2O_5 grown waveguide (400 nm grown)	5	1	2013 [6]
Strip loaded rib waveguide	5.8 (TE) 14 (TM)	6	2015 [19]
Wet Etched Ridge Waveguide	7 (TE) 6 (TM)	1	2015 [20]
Etched Ridge Waveguide (RIE and wet etching)	5	5	2016 [21]
Optical Dicing	1.2 (TE) 2.8 (TM)	2.1	2016 [22]
Etched Waveguide	0.33 (TE) 2.8 (TM)	5	This Work
Etched Waveguide	0.268 (TE) 1.3 (TM)	7	This Work

In summary, we developed and optimized fabrication processes that allow relatively smooth sidewall etching in lithium niobate. The reduction in sidewall roughness is reflected in electron microscope images as well as propagation loss measurements. To our knowledge, we currently have the lowest reported etched ridge waveguide losses of 0.33 dB/cm for a 5 μm waveguide with a deep etching of 700 nm. This demonstrates the practicability of lithium niobate on insulator as a platform for integrated optics, and compact structures with low loss can potentially be realized. While we have reached the threshold of under 1 dB/cm propagation loss, there is still much room for improvement as currently commercialized titanium diffused waveguides typically exhibit losses of under 0.086 dB/cm [8]. Additionally, the low coupling efficiency at the input side due to the submicron dimensions of these waveguides results in higher total insertion loss. Notwithstanding the engineering challenges ahead, we believe that this is very promising for the future of integrated optics.

Funding

Singapore National Research Foundation (NRF-CRP15-2015-01); PHC (Partenariat Hubert Curien) Merlion program (3.03.15).

Optics EXPRESS

Acknowledgments

The authors would like to thank David Troadec (IEMN) for his help with focused ion beam etching.